Monatshefte für Chemie (2002)
DOI 10.1007/s00706-002-0508-5

Monatshefte für Chemie
Chemical Monthly
Printed in Austria

Polymorphism and Pressure Driven Thermal Spin Crossover Phenomenon in [Fe(*abpt*)$_2$(NC*X*)$_2$] (*X* = S, and Se): Synthesis, Structure and Magnetic Properties

Ana B. Gaspar[1], **M. Carmen Muñoz**[2], **Nicolás Moliner**[1], **Vadim Ksenofontov**[3], **Georgii Levchenko**[4], **Philipp Gütlich**[3], and **José Antonio Real**[1,*]

[1] Departament de Química Inorgánica/Institut de Ciència Molecular, Universitat de València, Doctor Moliner 50, E-46100 Burjassot, València, Spain
[2] Departament de Física Aplicada, Universitat Politècnica de València, Camino de Vera s/n, E-46071 València, Spain
[3] Institut für Anorganische und Analytische Chemie, Johannes Gutenberg Universität, Staudinger Weg 9, D-55099 Mainz, Germany
[4] Donetsk Physico-Thecnical Institute, NAS of Ukraine, R. Luxemburg 72, UA-83114 Donetsk, Ukraine

Received June 12, 2002; accepted July 1, 2002
Published online November 7, 2002

Summary. The monomeric compounds [Fe(*abpt*)$_2$(NC*X*)$_2$] (*X* = S (**1**), Se (**2**) and *abpt* = 4-amino-3,5-bis(pyridin-2-yl)-1,2,4-triazole) have been synthesized and characterized. They crystallize in the monoclinic P2$_1$/n space group with $a = 11.637(2)$ Å, $b = 9.8021(14)$ Å, $c = 12.9838(12)$ Å, $\beta = 101.126(14)°$, and $Z = 2$ for **1**, and $a = 11.601(2)$ Å, $b = 9.6666(14)$ Å, $c = 12.883(2)$ Å, $\beta = 101.449(10)°$, and $Z = 2$ for **2**. The unit cell contains a pair mononuclear [Fe(*abpt*)$_2$(NC*X*)$_2$] units related by a center of symmetry. Each iron atom, located at a molecular inversion center, is in a distorted octahedral environment. Four of the six nitrogen atoms coordinated to the Fe(II) ion belong to the pyridine-N(1) and triazole-N(2) rings of two abpt ligands. The remaining *trans* positions are occupied by two nitrogen atoms, N(3), belonging to the two pseudo-halide ligands. The magnetic susceptibility measurements at ambient pressure have revealed that they are in the high-spin range in the 2 K–300 K temperature range. The pressure study has revealed that compound **1** remains in high-spin as pressure is increased up to 4.4 kbar, where an incomplete thermal spin crossover appears at around $T_{1/2} = 65$ K. Quenching experiments at 4.4 kbar have shown that the incomplete character of the conversion is a consequence of slow kinetics. Relatively sharp spin transition takes place at $T_{1/2} = 106$, 152 and 179 K, as pressure attains 5.6, 8.6 and 10.5 kbar, respectively.

* Corresponding author. E-mail: jose.a.real@uv.es

Keywords. Iron(II) complexes; Spin crossover; Polymorphism; X-ray structure determination; Pressure-induced spin transition.

Introduction

The spin crossover phenomenon deals with molecular materials that undergo phase transitions induced by temperature and/or pressure, as well as by light irradiation. The phase transition provokes drastic changes in their magnetic and optical properties conferring them a bistable character, which could be useful for the design of molecular devices [1]. Most spin crossover compounds are constituted by metallic ions with $3d^4$–$3d^7$ electronic configurations in pseudo-octahedral surroundings. Generally, two different arrangements for the d electrons, in the e_g and t_{2g} orbital subsets, may be envisaged according to whether the magnitude of the ligand field strength is smaller or greater than the mean inter-electronic repulsion energy. In the former case the 3d electrons adopt the high-spin (HS) configuration in order to minimize the inter-electronic repulsion. In the latter case the ligand field counter-balance the inter-electronic repulsion and the fundamental state becomes the low-spin state (LS) violating the *Hund*'s rule of maximum spin multiplicity. For intermediate ligand field strengths, a reversible thermal spin conversion between the LS ground state and the HS excited state may be observed when the energy difference between the HS state and the LS state is close to thermal energy. Then, an intra-ionic electron transfer takes place between the e_g and t_{2g} orbitals. Because the antibonding nature of the e_g orbitals, population and depopulation of these orbitals provokes a structural reorganization both at the molecular and the crystalline level. At the molecular level the main structural feature involves the metal-to-ligand bond distances change, being 0.1–0.2 Å shorter in the LS state.

The thermal spin crossover phenomenon is an entropy-driven process [2, 3]. Entropy stems from the difference in spin multiplicity and in vibrational density of the LS and HS states. Hence, at high temperatures molecules have sufficient energy as to populate nearly completely the HS excited state. In contrast, in a piezo-induced spin conversion the increase of pressure makes the metal-to-ligand bond distances shorter and, consequently, destabilizes the HS state in favour of the LS state.

Recently, we have reported the structural, magnetic, calorimetric and photomagnetic characterization of the spin crossover system $[Fe(abpt)_2(NCX)_2]$ ($X = S$ (**3**), Se (**4**), and NCN (**5**) prepared in methanol–chloroform solutions; *abpt* = 4-amino-3,5-bis(pyridin-2-yl)-1,2,4-triazole system [4, 5]. Compounds **3** and **4** are isostructural as they crystallize in the $P2_1/n$ space group and present very similar crystal and molecular parameters. The iron atom is surrounded by two abpt ligands, which occupy the equatorial positions, while the pseudohalide ligands complete the remaining positions of the $[FeN_6]$ core. Compound **5** crystallizes in the triclinic P-1 space group. Despite this difference the crystal packing is not very different to that of **3** and **4**. In fact, the $[Fe(abpt)_2(NCX)_2]$ mononuclear units interact via π-stacking defining infinite chains, which self-organize to define parallel sheets, in the three compounds. Compounds **3** and **4** undergo thermal induced spin conversion at $T_{1/2} = 180$ (1) and 224 (2) K. $T_{1/2}$ is the temperature at 50% of spin conversion where the number of HS and LS molecules is the same. Compound

5 undergoes a two-step spin transition at very low temperature ($T_{1/2} = 86$ K). Light-induced excited spin-state trapping (LIESST) is observed when irradiating samples of **3**–**5** with green light at 10 K.

During the synthesis of the red single crystals of **3** and **4** the simultaneous crystallization of a second type of orange single crystals was observed depending on the nature of the solvent we used. For instance, methanol–chloroform solutions of abpt and Fe/NCX^- (1:2) usually afforded **3** and **4**, while in methanol–water mixtures the main compound was an orange form, compounds **1** (S) and **2** (Se). Both kinds of compounds can be easily separated by hand with the help of binocular lens. Their chemical analyses, crystal diffraction patterns, and magnetic properties indicate that we were faced with two different polymorphs of $[Fe(abpt)_2(NCX)_2]$ with $X = S$, and Se. In the following text compounds **3** and **4** represent the polymorphs A and compounds **1** and **2** correspond to the polymorphs B. In this report we present and discuss the synthesis, the crystal structure and the thermal dependence of the magnetic properties of the polymorphs B at different pressures.

Results

*Crystal Structure of [Fe(abpt)$_2$(NCX)$_2$] (X = S (**1**), Se (**2**))*

Compounds **1** and **2** crystallize in the monoclinic $P2_1/n$ space group (see Table 1). The unit cell contains a pair of mononuclear $[Fe(abpt)_2(NCX)_2]$ units related by a center of symmetry. Each iron atom, located at a molecular inversion center, is in a

Table 1. Crystallographic data for $[Fe(abpt)_2(NCX)_2]$ (*X*: S, Se)

Compound **1**			
empirical formula	$C_{26}H_{20}FeN_{14}S_2$	V, Å^3	1417.6(4)
fw	648.53	Z	2
space group	$P2_1/n$	T, K	293(2)
a, Å	11.601(2)	λ, Å	0.71073
b, Å	9.6666(14)	μ, mm^{-1}	0.725
c, Å	12.883(2)	ρ_{calc}, g/cm^3	1.519
α, deg	90	$R1$[a]	0.0405
β, deg	101.126(14)	$wR2$[a]	0.0984
γ, deg	90		
Compound **2**			
empirical formula	$C_{26}H_{20}FeN_{14}Se_2$	V, Å^3	1451.5(3)
fw	742.33	Z	2
space group	$P2_1/n$	T, K	293(2)
a, Å	11.637(2)	λ, Å	0.71073
b, Å	9.8021(14)	μ, mm^{-1}	3.072
c, Å	12.9838(12)	ρ_{calc}, g/cm^3	1.698
α, deg	90	$R1$[a]	0.0391
β, deg	101.449(10)	$wR2$[a]	0.0731
γ, deg	90		

[a] $R1 = \Sigma||F_o|-|F_c||/\Sigma|F_o|$; $wR2 = \Sigma[w(F_o^2 - F_c^2)^2/\Sigma[w(F_o^2)^2]]^{1/2}$. $w = 1/[\sigma^2(F_o^2) + (0.0522P)^2 + 0.1930P]$ where $P = (F_o^2 + 2F_c^2)/3$

distorted octahedral environment. Four of the six nitrogen atoms coordinated to the Fe(II) ion belong to the pyridine-N(1) and triazole-N(2) rings of two abpt ligands. The remaining trans positions are occupied by two nitrogen atoms, N(3), belonging to the two pseudo-halide ligands (see Fig. 1). Interatomic bond distances and angles are collected in Table 2. The Fe–N bond distances involving the pyridine

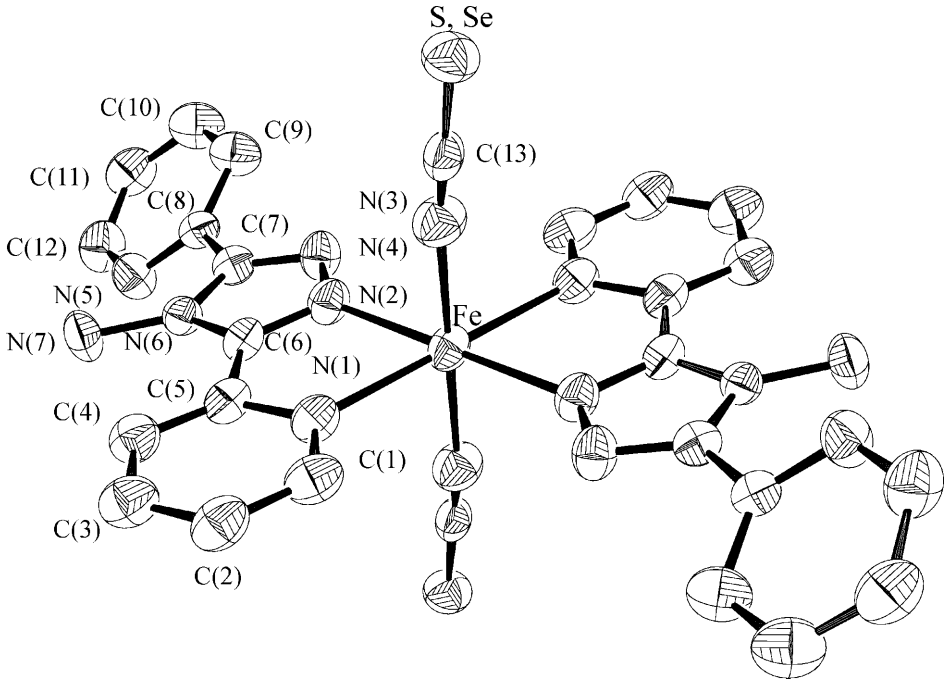

Fig. 1. Molecular structure of polymorphs B [Fe(*abpt*)$_2$(NC*X*)$_2$] (*X* = S, Se) at 293 K. Hydrogen atoms are omitted for clarity

Table 2. Selected bond distances (Å) and angles (deg)[a] for [Fe(*abpt*)$_2$(NC*X*)$_2$] (*X*: S, Se) polymorphs B

Compound **1**			
Fe–N(1)	2.226(4)	S(1)–C(13)	1.639(6)
Fe–N(2)	2.162(4)	N(3)–C(13)	1.165(6)
Fe–N(3)	2.125(5)	N(7)–H(7B)	0.90(6)
N(3)–C(13)	1.165(6)	N(7)–H(7A)	0.87(8)
N(1)–Fe–N(2)	75.18(14)	N(2)–Fe–N(3)	86.8(2)
N(1)–Fe–N(3)	89.2(2)	N(3)–C(13)–S(1)	179.7(5)
Compound **2**			
Fe–N(1)	2.217(5)	Se(1)–C(13)	1.798(7)
Fe–N(2)	2.171(5)	N(3)–C(13)	1.159(7)
Fe–N(3)	2.120(6)	N(7)–H(7B)	0.93(7)
N(3)–C(13)	1.159(7)	N(7)–H(7A)	0.79(6)
N(1)–Fe–N(2)	74.8(2)	N(2)–Fe–N(3)	86.9(2)
N(1)–Fe–N(3)	88.9(2)	N(3)–C(13)–Se(1)	179.3(6)

[a] Numbers in parentheses are estimated standard deviations in the least significant digit

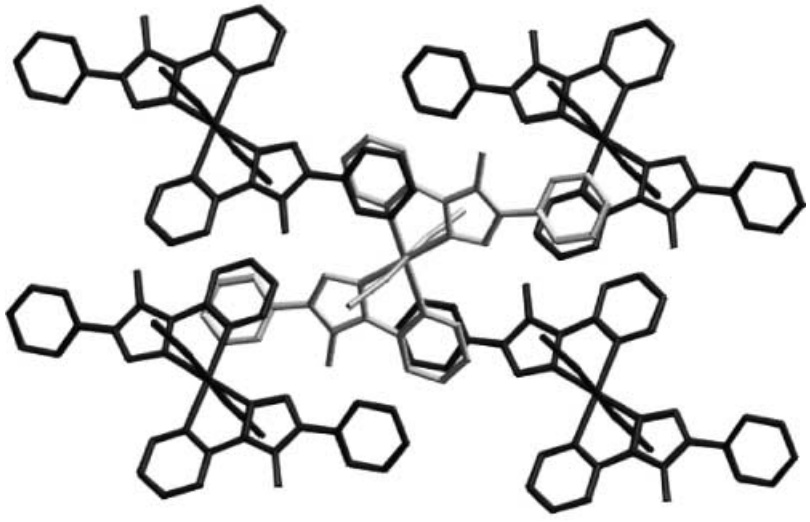

Fig. 2. Perspective view of the crystal packing of compounds **1** and **2**

ring (Fe–N(1) = 2.226(4) and 2.217(5) Å for **1** and **2**, respectively) are larger than those involving the triazole ring (Fe–N(2) = 2.162(4) and 2.171(5) Å for **1** and **2**, respectively) and the pseudo-halide groups (Fe–N(3) = 2.125(5) and 2.10(6) Å for **1** and **2**, respectively).

The NCX^- groups are almost linear (N(3)–C(13)–X = 179.7(5)° and 179.3(6)° for **1** and **2**, respectively) whereas the linkages Fe–NCX are bent (Fe–N(3)–C(13) = 169.6(4)° and 169.7(5)° for **1** and **2**, respectively). The coordinated pyridine and triazole rings almost remain in the same plane (dihedral angle 125.4(4)°). In contrast, the uncoordinated pyridine group and the chelate pyridine-triazole system define a dihedral angle of 34.6° (**1**) and 34.4° (**2**).

As can be seen in Fig. 2 the crystal packing of **1** and **2** is defined by the π-stacking of mononuclear [Fe(*abpt*)$_2$(NCX)$_2$] units. Each unit interacts with four surrounding neighbor units in such a way that the uncoordinated pyridine ring of one abpt ligand in [Fe(*abpt*)$_2$(NCX)$_2$] interacts with the coordinated pyridine ring of the adjacent [Fe(*abpt*)$_2$(NCX)$_2$] unit. The average distance between overlapping ligands is ca. 3.6 Å.

Magnetic Properties under Pressure

Figure 3 shows the temperature dependence of the $\chi_M T$ product for **1** (open rhombuses) and **2** (full rhombuses), χ_M being the molar magnetic susceptibility and T the temperature. At room temperature and $P = 1$ bar, $\chi_M T$ is equal to 3.68 and 3.79 $cm^3\,K\,mol^{-1}$ for **1** and **2** respectively, which is in the range of the values expected for an iron(II) ion in the HS state. As the temperature is lowered, $\chi_M T$ practically remains constant for both compounds, the dropping of $\chi_M T$ at temperatures below 25 K corresponds most probably to the occurrence of zero-field splitting of the HS iron(II) ions.

The magnetic properties of compound **1** were measured at different pressures in the range of temperatures 300–4.2 K. The $\chi_M T$ product is displayed in the Fig. 4 at

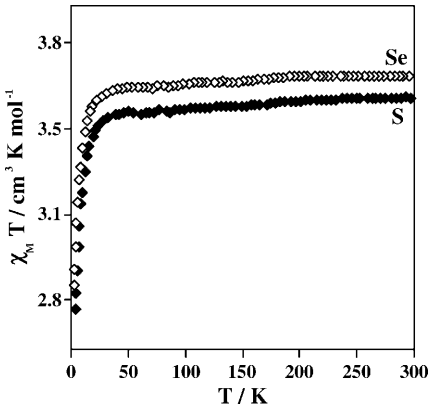

Fig. 3. $\chi_M T$ versus T plots for compounds **1** and **2**. Samples were cooled from 300 to 2 K at 2 K min^{-1}

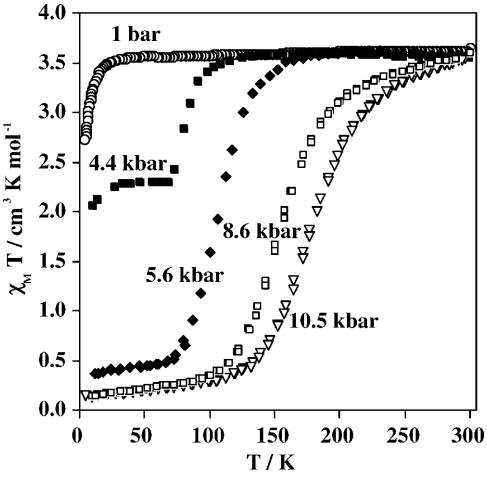

Fig. 4. Temperature dependence of $\chi_M T$ at different pressures for [Fe(*abpt*)$_2$(NCS)$_2$] polymorph B: 1 bar (open circles), 4.4 kbar (black squares), 5.6 kbar (black rhombuses), 8.6 kbar (open squares), 10.5 kbar (open triangles)

various pressures. Compound **1** does not reveal the spin crossover behaviour at ambient pressure and the iron(II) ion is in the HS state in the whole range of temperatures. This behaviour remains as pressure is increased up to 4.4 kbar, where an incomplete thermal spin crossover appears around $T_{1/2} = 65$ K. This $T_{1/2}$ value is one of the lowest temperatures observed for an iron(II) spin-crossover compound. Observation of considerable amounts of trapped HS molecules at low temperature is usually attributed to the occurrence of two different sites in the crystal [6]. One of the sites feels weaker ligand field strength and, consequently, stabilizes HS molecules whereas the other with stronger ligand field stabilizes spin-crossover centres. Texture effects or occurrence of different polymorphs, one of them being paramagnetic in the whole range of temperatures, has also been claimed [1b–d]. However, it is more reasonable to consider here that slow kinetics could block the HS–LS equilibrium, due to the low temperatures involved in the spin transition of

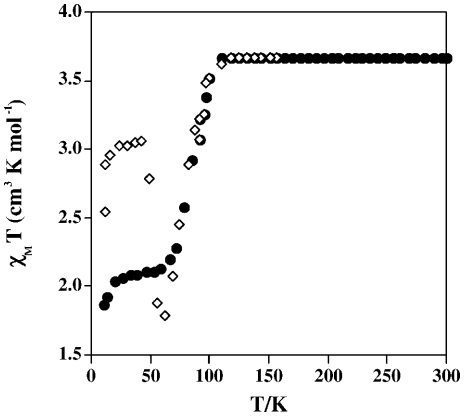

Fig. 5. $\chi_M T$ versus T plots for [Fe(*abpt*)$_2$(NCS)$_2$] polymorph B. Sample was cooled from 300 to 2 K at 2 K min^{-1} (black circles). Thermal quenching at 4.4 kbar: sample was cooled from 300 to 5 K at 100 K min^{-1} and then warmed slowly (open rhombuses, see text)

1 at 4.4 kbar. A relatively sharp spin transition takes place at $T_{1/2} = 106$, 152 and 179 K, as pressure attains 5.6, 8.6 and 10.5 kbar, respectively. In the slow cooling and heating modes with the rate 0.1 K min^{-1} providing the thermodynamic equilibrium conditions, the transitions are accompanied by a 2 K wide thermal hysteresis at all pressures studied.

Dynamics of the Spin Conversion. Thermal Quenching at 4.4 kbar

We have performed thermal quenching experiments at 4.4 kbar by cooling the sample rapidly (100 K min^{-1}) from room temperature down to 5 K to demonstrate that slow kinetics effects are present in **1**. Figure 5 displays the magnetic behaviour of the quenched sample at increasing temperatures. $\chi_M T$ is equal to 2.5 cm^3 K mol^{-1}, at 5 K. This value represents apparently 68% of trapped HS molecules. A progressive increase of $\chi_M T$ was observed as the sample was slowly warmed (2 K min^{-1}). The thermal dependence of $\chi_M T$ attains a maximum value of 3.0 cm^3 K mol^{-1} in the range of temperatures 20–40 K. The increase of $\chi_M T$ corresponds, most probably, to the occurrence of zero-field splitting in the $S = 2$ ground state of the trapped HS molecules. Hence, the effective thermal quenching at low temperatures actually involves around 84% of molecules in the HS state. In the range of temperatures 50–65 K, $\chi_M T$ diminishes as a consequence of HS–LS relaxation. In this range of temperatures, $\chi_M T$ was registered every 2 K after waiting sufficiently long at each temperature in order to reach thermodynamic equilibrium. The sequence with delays given in parentheses, was the following: 48 K (60 min), 50 K (120 min), 52 K (120 min), 54 K (60 min), 56 K (60 min), 58 K (30 min), 60 K (30 min) and 62 K (15 min). As can be seen in Fig. 5, $\chi_M T$ falls down to ca. 1.7 cm^3 K mol^{-1} at 62 K. Obviously, greater delays would produce smaller $\chi_M T$ values according to a greater extent of the HS-LS relaxation. For the temperatures higher than 62 K, the molecules overcome the energy barrier between the two LS and HS potential wells. Consequently, both, normal regime and thermal quenching experiments coincide above $T = 72$ K.

Discussion

Polymorphs B (compounds **1** and **2**) have a molecular structure very similar to that previously reported for [Fe(*abpt*)$_2$(NC*X*)$_2$] (*X* = S, Se), polymorphs A. The average Fe–N bond distances, R[FeN$_6$], are very similar in both polymorphs being larger for polymorph B (see Table 2). The main structural difference of **1** and **2** with respect to polymorphs A, is the intermolecular hydrogen bonding between the amine group of the triazole ring and the nitrogen atom of the uncoordinated pyridine ring that does not take place in the polymorphs B [4, 5, 7]. This is the reason why the crystal packing of **1** and **2** differs from that of polymorphs A. The absence of intramolecular hydrogen bonding in **1** and **2** favours the formation of two-dimensional nets stacking in the [101] direction. The cohesion force inside the plane is determined by the $\pi-\pi$ intermolecular interactions between the coordinate and uncoordinated pyridine rings.

The different crystal packing in polymorphs B with respect to polymorphs A, provokes that the Fe–N bond distances in **1** and **2** are longer than in **3** and **4**. This is probably due to steric hindrance induced by the proximity of the uncoordinated pyridine ring of the adjacent abpt ligand to the Fe–N bond of the coordinated pyridine group.

As previously reported [Fe(*abpt*)$_2$(NC*X*)$_2$] (*X* = S, Se), polymorphs A show thermal spin transition with $T_{1/2} = 180(1)$ and 224(2) K [4]. In contrast, the compounds **1** and **2** do not undergo spin transition, they remain in the HS state in the whole range of temperature. The thermal dependence of the magnetic properties of compound **1** has been studied at different pressures. The compound undergoes an incomplete thermal spin transition at 4.4 kbar. The trapping experiments have shown that, in the warming mode of the sample, at rates as slow as 0.028 K min^{-1} the metastable HS state relaxes back to the LS ground state. The relaxation takes place with greater efficiency than in the standard warming procedure where 62% of molecules remain in the HS state at low temperatures. For temperatures greater than 65 K the population of the HS state becomes more favourable and $\chi_M T$ increases. As pressure is increased the spin conversion becomes complete. It should be mentioned that the magnetic properties of **1** at 10.5 kbar are very similar to those of **3** at ambient pressure. Also, it should be noted the linear behaviour of the pressure dependence of $T_{1/2}$ for the spin conversion of **1** (see Fig. 6). The slope of the $T_{1/2}$ *vs P* straight line,

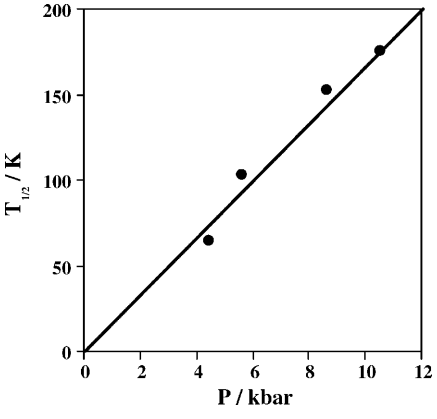

Fig. 6. $T_{1/2}$ versus *P* plot for **1**

$dT_{1/2}/dP = 17.6\,K\,kbar^{-1}$, is very close to that observed for the mononuclear compound $[Fe(2\text{-}pic)_3]Cl_2 \cdot EtOH$ (*2-pic* = 2-picolylamine) [8] where $dT_{1/2}/dP = 15\,K\,kbar^{-1}$. However, these values of $dT_{1/2}/dP$ are significantly smaller than those observed for the one-dimensional coordination spin crossover polymer $[Fe(hyetrz)_3]X_2 \cdot 3H_2O$ (*hyetrz* = 4-(2′-hydroxyethyl)-1,2,4-triazole, *X* = 3-nitrophenylsulphonate), which is around $24\,K\,kbar^{-1}$ [9].

Conclusion

We have reported here a new example of the effect of polymorphism on the spin transition. Two crystal forms, so-called polymorphs A and B, of the same complex exhibit different magnetic properties: polymorphs A undergo thermal spin transition at ambient pressure while polymorphs B are paramagnetic in the whole range of temperature at 1 bar, however, they undergo thermal spin transition at higher pressures. Comparison of the crystal structures of the two polymorphs showed that the differences are mostly due to crystal packing effects rather than to changes in the complex geometry, even though small differences in the Fe–N intramolecular distances and in the conformations of the chelate rings have been evidenced.

Experimental

4-amino-3,5-bis(pyridin-2-yl)-1,2,4-triazole (Aldrich), $FeSO_4 \cdot 7H_2O$ (Panreac) and KNC*X* (*X* = S, Se) (Aldrich) where purchased from commercial sources and used as received.

*[Fe(abpt)$_2$(NCX)$_2$] (X = S (**1**), Se (**2**))*

To a solution of abpt (0.5 mmol, 119 mg) in methanol (20 ml) was added a water/methanol (1:1) solution (40 ml) of $FeSO_4 \cdot 7H_2O$ (0.25 mmol). The resulting solution was mixed with a solution of KNC*X* (*X* = S, Se) (0.5 mmol of KNC*X*) in water (20 ml). The final orange solution was filtered and allowed to evaporate for a week, giving orange crystals of **1** and **2** suitable for X-rays studies. All manipulations were performed in an argon atmosphere. Yield = 60%. Anal. calc. for $C_{26}H_{20}N_{14}S_2Fe$ (**1**): C 48.16, H 3.09, N 30.25; found: C 47.95, H 3.07, N 30.08. Anal. calc. for $C_{26}H_{20}N_{14}Se_2Fe$ (**2**): C 42.06, H 2.69, N 26.42; found: C 42.58, H 2.62, N 25.98.

Crystallographic Data

Diffraction data for compounds **1** and **2** were collected at room temperature with an Enraf-Nonius CAD-4 diffractometer using graphite monochromated Mo Kα radiation with the $\omega - 2\theta$ scan method (see Table 1). The unit cell parameters were determined from least squares refinement on the setting angles from 25 centered reflections in the range $12 < \theta < 20°$. No significant fluctuations were observed in the intensities of three standard reflections monitored periodically throughout data collections. The structures were solved by standard *Patterson* methods and refined by the full-matrix least-squares method on F^2. The computations were performed by using SHELXS97 and SHELXL97 [10]. All non-hydrogen atoms were refined anisotropically. The final full-matrix least-squares refinement, minimizing $\Sigma[w(F_o^2 - F_c^2)^2]$ converged at the values of *R*1 and *wR*2 are listed in Table 1. The molecular plots were drawn with the ORTEP program [11].

Magnetic Susceptibility Measurements

The variable-temperature magnetic susceptibility measurements at atmospheric pressure were carried out on microcrystalline samples using a Quantum Design MPMS2 SQUID susceptometer equipped

with a 55 kG magnet and operating in the range 0.1–1T and 1.8–300 K. The susceptometer was calibrated with $(NH_4)Mn(SO_4)_2 \cdot 12H_2O$. The set of magnetic measurements performed at variable pressure was carried out in the temperature range 5–320 K on a Foner magnetometer (Pricenton Applied Research PAR 151) equipped with a Bruker electromagnet operating at 1T and a CryoVac liquid helium cryostat. A prototype of the actual construction of a hydrostatic high-pressure cell (HPC) made of hardened beryllium bronze with silicon oil as a pressure-transmitting media was described elsewhere [12, 13]. The cell has the following characteristics: weight 8 g, range of pressure up to 13 kbar, accuracy $\pm$ 0.25 kbar, nonhydrostaticity of pressure is less than 0.5 kbar, sample space is 1 mm in diameter and 5–7 mm in length. The pressure was calibrated using the transition temperature of superconducting tin of purity 99.99%. Experimental susceptibilities were corrected for diamagnetism of the constituent atoms by the use of *Pascal*'s constants.

Acknowledgements

This work was funded by the European Commission trough TMR-Network "Thermal and Optical Switching of Spin States (TOSS)", Contract No. ERB-FMRX-CT98-0199EEC/TMR, the Deutsche Forschungsgemeinschaft, Schwerpunktprogramm "Molekularer Magnetismus", the Fonds der Chemischen Industrie and the Ministerio Español de Ciencia y Tecnología (project BQU 2001-2928).

References

[1] a) Goodwin HA (1976) Coord Chem Rev **18**: 293; b) Gütlich P (1981) Struct Bonding (Berlin) **44**: 83; c) Gütlich P, Hauser A, Spiering H (1994) Angew Chem Int Ed Engl **33**: 2024; d) König E, Ritter G, Kulshreshtha SK (1985) Chem Rev **85**: 219; e) König E (1991) Struct Bonding (Berlin) **76**: 51; f) Lawthers I, McGarvey JJ (1984) J Am Chem Soc **106**: 4280; g) Decurtins S, Gütlich P, Hasselbach KM, Spiering H, Hauser A (1985) Inorg Chem **24**: 2174; h) Decurtins S, Gütlich P, Köhler CP, Spiering H, Hauser A (1984) Chem Phys Lett **105**: 1

[2] Sorai M, Seki S (1974) J Phys Chem Solids **35**: 555

[3] Slichter CP, Drickamer HG (1972) J Chem Phys **56**: 2142

[4] Moliner N, Muñoz MC, Létard S, Létard J-F, Solans X, Burriel R, Castro M, Kahn O, Real JA (1999) Inorg Chim Acta **291**: 279

[5] Moliner N, Gaspar AB, Muñoz MC, Niel V, Cano J, Real JA (2001) Inorg Chem **40**: 3986

[6] a) Poganiuch P, Decurtins S, Gütlich P (1990) J Am Chem Soc **112**: 3270; b) Poganiuch P, Gütlich P (1988) Hyperfine Interact **40**: 331; c) Buchen T, Poganiuch P, Gütlich P (1994) J Chem Soc, Dalton Trans 2285; d) Hinek R, Spiering H, Schollmeyer D, Gütlich P, Hauser A (1996) Chem Eur J **2**: 1127

[7] a) Cornelissen JP, Diemen JH, Groeneveld LR, Haasnoot JG, Spek AL (1992) Inorg Chem **31**: 198; b) Faulmann C, Koningsbruggen PJ, Graaff RAG, Haasnoot JG, Reedijk J (1990) Acta Crystallogr **C46**: 2357; c) García MP, Manero JA, Oro LA, Apreda MC, Cano FH, Foces-Foces C, Haasnot JG, Prins R, Reedijk J (1986) Inorg Chim Acta **122**: 235

[8] Köhler CP, Jakobi R, Meissner E, Wiehl H, Spiering H, Gütlich P (1990) J Phys Chem Solids **51**: 239

[9] Garcia Y, Van Koningsbruggen P, Lapouyade R, Fournés L, Rabardel L, Kahn O, Ksenofontov V, Levchenko G, Gütlich P (1998) Chem Mater **10**: 2426

[10] Sheldrick GM, SHELXS97 (1990) Acta Crystallogr **A46**: 467; SHELXL97 (1997) Program for the Refinement of Crystal Structures, Univ of Götingen, Germany

[11] Johnson CK, ORTEP (1971) Report ORNL-3794, Oak Ridge National Laboratory, Oak Ridge, TN

[12] Dyakonov VP, Levchenko G (1983) Sov J Pribori Texnika Experimenta **5**: 236

[13] Baran M, Levchenko G, Dyakonov VP, Shymchack G (1995) Physica **C241**: 383